Small-Signal Stability Analysis and Optimal Parameters Design of Microgrid Clusters

He, Jinghan; Wu, Xiaoyu; Wu, Xiangyu; Xu, Yin; Guerrero, Josep M.

Published in:
IEEE Access

DOI (link to publication from Publisher):
10.1109/ACCESS.2019.2900728

Publication date:
2019

Document Version
Publisher's PDF, also known as Version of record

IEEE Access
Multidisciplinary | Rapid Review | Open Access Journal

Received January 16, 2019, accepted January 28, 2019, date of publication February 22, 2019, date of current version April 3, 2019.

Digital Object Identifier 10.1109/ACCESS.2019.2900728

Small-Signal Stability Analysis and Optimal Parameters Design of Microgrid Clusters

JINGHAN HE[1], (Senior Member, IEEE), XIAOYU WU[1], (Student Member, IEEE), XIANGYU WU[1], (Member, IEEE), YIN XU[1], (Senior Member, IEEE), AND JOSEP M. GUERRERO[2], (Fellow, IEEE)

[1]School of Electrical and Engineering, Beijing Jiaotong University, Beijing 100044, China
[2]Department of Energy Technology, Aalborg University, 9220 Aalborg, Denmark

Corresponding author: Xiangyu Wu (wuxiangyu@bjtu.edu.cn)

This work was supported in part by the National Key R&D Program of China under Grant 2017YFB0903005, in part by the National Natural Science Foundation of China under Grant 51807004 and Grant 51807005, and in part by the China Postdoctoral Science Foundation under Grant 2017M620600.

ABSTRACT The two-layer distributed control architecture, including the microgrid (MG) control layer and MG cluster (MGC) control layer, can be used for interconnecting multiple MGs to form the MGC. However, the coupling among multiple elements and the interaction between two control layers may introduce new low-damping oscillatory modes and even reduce the stability margin. Unfortunately, the detailed small-signal stability analysis and stability enhancement method of the MGC with the two-layer distributed control strategy have not been reported. To fill this gap, this paper first presents a unified small-signal dynamic model of the MGC. Subsequently, a comprehensive small-signal stability analysis based on the model is presented to analyze: 1) the mechanism of coupling/interaction among MGs and multiple control layers; 2) the participation factors of the low-damping modes; and 3) the sensitivity of the distributed control parameters. Moreover, the design of the distributed control parameters is formulated as an optimization problem, where the particle swarm optimization is employed to search for an optimal combination of parameters to enhance system stability. Finally, the stability assessment and time-domain simulation are carried out to validate the effectiveness of the proposed method.

INDEX TERMS Distributed control, hierarchical control, microgrid cluster, particle swarm optimization, small-signal stability.

I. INTRODUCTION

In recent years, the microgrid (MG) has experienced rapid development because it is an effective solution for the reliable integration of distributed generation (DG) units, energy storage systems, and loads [1]–[3]. Meanwhile, with the increasing application of MGs, interconnecting MGs to form a microgrid cluster (MGC) is considered as an effective option of enabling maximum utilization of renewable sources, suppressing stress and aging of the components in MGs [4] or even operating as an island to serve more area when a major outage happened [5].

The three-level hierarchical control architecture including primary control, secondary control and tertiary control is widely investigated for a single MG to realize its voltage/frequency regulation, power balance and load sharing [6], [7]. However, for a MGC, the two-layer architecture is commonly adopted, in which the classical MG three-level control is modified and embedded into the MG-control layer, and a MGC-control layer is employed to overlook the resources and realize coordination of multiple MGs [8]–[10]. For the two-layer control architecture of MGC, there are centralized or distributed ways to perform the control actions. Due to the advantages of reliability, reconfigurability and low communication investment, the distributed control method gains a lot of concerns for the MGC [11]–[15]. Based on the distributed communication network, each DG unit or MG unit only requires its own and the neighbor's information to realize control objectives. The existing two-layer distributed control methods for the MGC mainly focus on realization of the steady-state objectives, e.g., (i) elimination of system frequency deviations [12], [15], (ii) regulation of system voltage,

The associate editor coordinating the review of this manuscript and approving it for publication was Jagdish Chand Bansal.

such as DG units AC-side voltages or critical bus voltage [13], and (iii) accurate power sharing among MGs [11], [14].

However, the dynamic characteristics of the MGC may be undesirable in terms of the system damping, response time, stability margin and so on [16], [17]. First, the interaction between two control layers and the dynamic coupling among multiple MGs may introduce new low-damping modes, which lead to oscillatory responses or even destabilize the system. Moreover, compared with the centralized method, the neighboring communication characteristic of the distributed control method may result in a more significant interaction/coupling among DG or MG units. Therefore, a detailed small-signal stability analysis for the MGC is of significant importance. In [16], a small-signal modeling method for the MGC is proposed, in which each MG is simplified as a DG unit without considering its internal dynamics. Thus, the simplification in [16] will inevitably lead to analysis errors. In [17], a detailed small-signal dynamic model of a PV-based MGC is proposed and the analysis results indicate that the coupling among MGs will weaken the system stability. However, only decentralized primary control is employed with each DG in [17], which means the impact of other control layers, especially the impact of interaction between different control layers cannot be studied. To the best of our knowledge, a comprehensive small-signal stability analysis of the MGC considering detailed models and distributed control method has not been reported before.

Furthermore, although many methods have been proposed to enhance the stability of a single MG [18]–[21], to the best of our knowledge, the stability enhancement via optimal control parameters design for the MGC has not been reported before. Compared with a single MG, the complicated interactions/couplings in a MGC with the two-layer distributed control strategy are strongly associated with multiple control parameters. Therefore, the control parameters of both the MGC and MG control layer should be optimized jointly.

Motivated by the aforementioned limitations, this paper focuses on stability analysis and enhancement method of the MGC with the two-layer distributed control strategy. The main contributions of this paper include:

1) a comprehensive stability analysis of the MGC based on its small-signal dynamic model to reveal the coupling mechanism among multiple MGs, control interaction between different control layers and the impact of control parameters on stability;
2) a formulation of the control parameters optimal design problem considering both MG-control layer and MGC-control layer and a particle swarm optimization (PSO) approach to jointly optimize multiple control parameters to enhance the system stability.

This paper also presents time-domain simulation validations of the MGC small-signal dynamic model to ensure an accurate and reliable stability analysis result. Eigenvalue analysis and time-domain simulation are provided to verify the effectiveness of the proposed parameters optimization method.

The rest of the paper is organized as follows. Section II describes the unified small-signal dynamic model of the MGC with the two-layer distributed control method. Section III presents the stability analysis of the MGC based on the small-signal dynamic model. Section IV formulates the control parameters optimization problem and the PSO based solution method. Case studies are presented in Section V to validate the effectiveness and of the proposed stability enhancement method. Section VI concludes the paper.

II. SMALL-SIGNAL DYNAMIC MODEL OF THE MGC WITH THE TWO-LAYER DISTRIBUTED CONTROL STRATEGY

In this section, the two-layer distributed control method for the MGC is presented. Based on it, the small-signal dynamic model is provided.

A. TWO-LAYER DISTRIBUTED CONTROL FRAMEWORK FOR MGC

The two-layer distributed control framework includes (i) primary and distributed secondary control levels in the MG-control layer, (ii) tertiary and distributed quaternary control levels in the MGC-control layer.

- The primary control (PC) level is responsible for controlling the local power, voltage, and current of DGs.
- The distributed secondary control (DSC) level is introduced to adjust the voltage phasor of the point of common coupling (PCC) in the MG by controlling the PCC voltage magnitude and frequency at the reference values received from the tertiary control level.
- The tertiary control (TC) level manages the power flow through PCC of each MG by sending commands to the secondary control level.
- The distributed quaternary control (DQC) level supervises the entire MGC and controls the critical bus voltage and system frequency as desired values.

A schematic diagram of the two-layer distributed control framework is presented in Fig. 1.

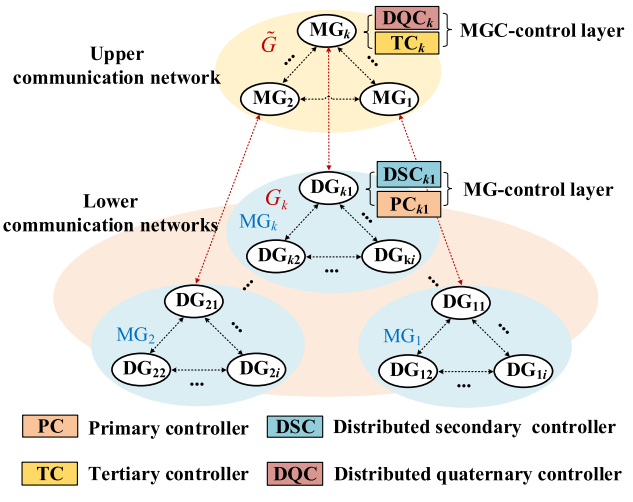

FIGURE 1. Two-layer distributed control architecture of the MGC.

Within an arbitrary MG_k, each DG unit communicates with its neighbors to formulate the lower distributed communication network G_k. Then, each MG is represented by an agent and communicates with its neighbors to formulate the upper distributed communication network $\tilde{G}$. Note that each MG agent needs to communicate with at least one DG unit inside this MG, as shown by the red dashed lines in Fig. 1, to realize the coordination between two control layers.

The corresponding control objectives are summarized as follows:

(i) The system frequency $\omega_{\rm sys}$ is controlled as the desired value $\omega^*_{\rm sys}$.

(ii) The critical bus voltage $V_{\rm c}$ is restored to the desired value $V^*_{\rm c}$. Note that the critical bus can be selected according to the operation requirement and only one critical bus is selected in this paper.

(iii) The active and reactive power through PCC of each MG are shared among them based on their capacities, i.e.,

$$P_{\rm PCC1}/P_{\rm mMG1} = \ldots = P_{\rm PCC}m/P_{\rm mMG}m \quad (1)$$

$$Q_{\rm PCC1}/Q_{\rm mMG1} = \ldots = Q_{\rm PCC}m/Q_{\rm mMG}m \quad (2)$$

where $P_{\rm mMGk}$, $Q_{\rm mMGk}$, $P_{\rm PCCk}$, $Q_{\rm PCCk}$ are active and reactive power capacities of MG_k, output active and reactive power through PCC_k, respectively, with $k \in \mathcal{M}$, $\mathcal{M} = \{1, 2, \ldots, m\}$.

(iv) Within each MG, the output active and reactive power of each DG are shared among them based on their power capacities, i.e.,

$$P_{k1}/P_{\rm mk1} = \ldots = P_{kn_k}/P_{\rm mkn_k} \quad (3)$$

$$Q_{k1}/Q_{\rm mk1} = \ldots = Q_{kn_k}/Q_{\rm mkn_k} \quad (4)$$

where $P_{\rm mki}$, $Q_{\rm mki}$, P_{ki}, Q_{ki} are active and reactive power capacities, output active and reactive power of DG_i in MG_k, respectively, with $i \in \mathcal{N}_k$, $\mathcal{N}_k = \{1, 2, \ldots, n_k\}$.

B. MG LAYER CONTROLLERS AND SMALL-SIGNAL DYNAMIC MODELING

In the MG-control layer, the droop method is adopted as the primary control. The distributed secondary control is designed based on distributed cooperative control [22], [23] and then implemented through the communication network G_k which is modeled by a digraph in the graph theory [24]. The associated adjacency matrix with G_k is $\mathbf{A}^k = \left[a^k_{ij}\right]$. Assume for an arbitrary MG_k, the internal DG units are considered as nodes in G_k, as shown in Fig. 1.

1) PRIMARY CONTROLLER (PC) AND DISTRIBUTED SECONDARY CONTROLLER (DSC)

The PC is based on the droop method [25], [26] which consists of the power controller, inner voltage controller, and current controller, as shown in Fig. 2. The power controller is

$$\omega_{ki} = \omega_{\rm n} - D_{{\rm P}ki}P_{ki} + \Omega_{ki} \quad (5)$$

$$E_{{\rm od}ki} = V_{\rm n} - D_{{\rm Q}ki}Q_{ki} + \lambda_{ki} + h_{ki} \quad (6\text{-a})$$

$$E_{{\rm oq}ki} = 0 \quad (6\text{-b})$$

where ω_{ki} is the angular frequency of DG_i in MG_k, $\omega_{\rm n}$ is the rated angular frequency, $V_{\rm n}$ is the rated voltage of the low voltage (LV) network. $E_{{\rm od}ki}$ is the d-axis voltage reference, and the q-axis voltage reference $E_{{\rm oq}ki}$ is set to be zero. $E_{{\rm od}ki}$ and $E_{{\rm oq}ki}$ are provided to the inner voltage controller. $D_{{\rm P}ki}$ and $D_{{\rm Q}ki}$ are active and reactive power droop coefficients, respectively. Ω_{ki}, λ_{ki} and h_{ki} are the distributed secondary control variables.

The DSC is based on a distributed frequency and voltage control method for MG introduced in our previous work [27]. More details can be found in [27]. The only modification of the DSC in this paper is controlling the angular

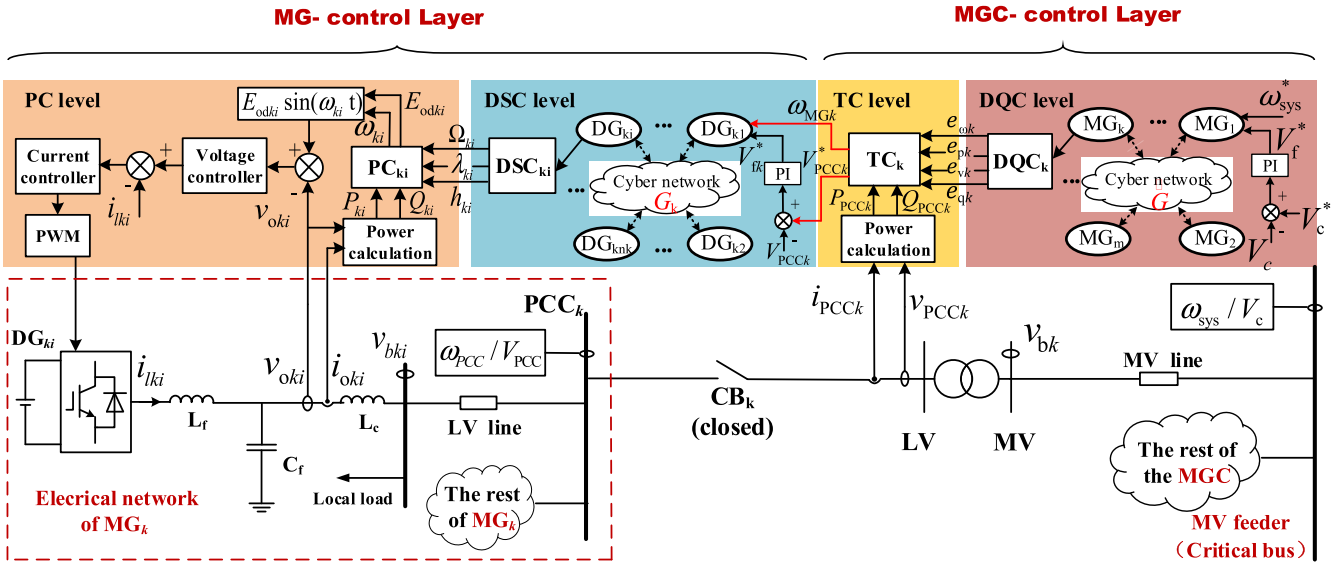

FIGURE 2. A block diagram of the two-layer distributed control method.

frequency ω_{PCC} and PCC voltage V_{PCC} as $\omega_{\mathrm{MG}k}$ and $V^*_{\mathrm{PCC}k}$ received from the TC instead of controlling them as rated frequency and voltage in [27]. This modification can embed the MG-layer control into the overall control architecture of the MGC.

2) SMALL-SIGNAL DYNAMIC MODEL OF MG_K

The reference frame of DG_{11}, namely DG_1 in MG_1, is selected as the common DQ-frame of the entire MGC. Thus, the phase angle δ_{ki} of DG_{ki} can be defined as

$$\dot{\delta}_{ki} = \omega_{ki} - \omega_{\mathrm{g}} \tag{7}$$

where ω_g is the rotating frequency of the common DQ-frame and equal to ω_{11}, and ω_{ki} is the rotating frequency of local dq-frame of DG_{ki}.

By modeling the dynamics of PCs, DSCs, lines and loads inside MG_k, the model of MG_k can be obtained [27], i.e.,

$$\left[\Delta\dot{S}_{\mathrm{MG}k}\right] = A_{\mathrm{MG}k}\left[\Delta S_{\mathrm{MG}k}\right] + B_{\mathrm{MG}k}\Delta V^*_{\mathrm{PCC}k} + C_{\mathrm{MG}k}\left[\Delta i_{\mathrm{PCCDQ}k}\right] \tag{8}$$

where $\Delta S_{\mathrm{MG}k} = [\Delta X_{\mathrm{DG}k}, \Delta i_{\mathrm{lineDQ}k}, \Delta i_{\mathrm{loadDQ}k}, \Delta\psi_k]^T$, $\Delta X_{\mathrm{DG}k}$ refers to the state variables of all DG units in MG_k and $\Delta X_{\mathrm{DG}k} = [\Delta X_{\mathrm{DG}k1}, \Delta X_{\mathrm{DG}k2}, \ldots, \Delta X_{\mathrm{DG}kn_k}]^T$, $\Delta X_{\mathrm{DG}ki} = \left[\Delta\delta_{ki}, \Delta P_{ki}, \Delta Q_{ki}, \Delta\Omega_{ki}, \Delta\lambda_{ki}, \Delta h_{ki}, \Delta i_{\mathrm{odq}ki}\right]^T$, $i_{\mathrm{od}ki}$, $i_{\mathrm{oq}ki}$ are the d-axis and q-axis component of DG output current $i_{\mathrm{o}ki}$ in Fig.2. $\Delta\psi_k$ is a state variable introduced by the PCC voltage controller, $\Delta V^*_{\mathrm{PCC}k}$ and $\Delta i_{\mathrm{PCCDQ}k}$ are coupling states which reflect the interactions among the MG_k and other MGs. $A_{\mathrm{MG}k}$, $B_{\mathrm{MG}k}$ and $C_{\mathrm{MG}k}$ are parameter matrices. Therefore, as indicated by (8), the dynamics of PCs, DSCs, loads and lines are modeled and the detailed modeling process can be found in [27].

C. MGC LAYER CONTROLLERS AND SMALL-SIGNAL DYNAMIC MODELING

In the MGC-control layer, the TCs and DQCs are employed to realize objective (i) - (iii).

1) TERTIARY CONTROLLER (TC)

The TC is a local controller which is responsible for regulating the active and reactive power through PCC of each MG. To ensure the plug-and-play characteristic of MGs, each MG is considered as a droop-controlled node, given by,

$$\omega_{\mathrm{MG}k} = \omega_n - D_{\mathrm{P}k}P_{\mathrm{PCC}k} \tag{9}$$

$$\hat{V}_{\mathrm{PCC}k} = V_n - D_{\mathrm{Q}k}Q_{\mathrm{PCC}k} \tag{10}$$

where $\omega_{\mathrm{MG}k}$ and $\hat{V}_{\mathrm{PCC}k}$ are the angular frequency and voltage reference values, $D_{\mathrm{P}k}$ and D_{Qk} are the active and reactive droop coefficients of MG_k, respectively, determined by

$$D_{\mathrm{P}k} = \Delta\omega_{max}/P_{\mathrm{mMG}k}, D_{\mathrm{Q}k} = \Delta V_{max}/Q_{\mathrm{mMG}k} \tag{11}$$

where $\Delta\omega_{max}$ and ΔV_{max} are the maximum acceptable angular frequency and PCC voltage magnitude deviations, respectively.

2) DISTRIBUTED QUATERNARY CONTROLLER (DQC)

The DQC is responsible for regulating system frequency and critical bus voltage to the desired values. Besides, the inaccurate reactive power sharing problem due to unbalanced line impedance [28] is solved by DQC. The DQC is designed based on the concept of the distributed cooperative control [22], [23]. The communication network is denoted as $\tilde{G}$ with the associated adjacency matrix $\mathbf{A} = [\tilde{a}_{kl}]$. Each MG is considered as a node in $\tilde{G}$, as shown in Fig.1. For node k, the set of its neighbors is denoted as H_k.

The *frequency/active power controller* of DQC level aims at realizing objective (i) and (iii)-(1). The control variable Ω_k is introduced on (9), given by

$$\omega_{\mathrm{MG}k} = \omega_{\mathrm{n}} - D_{\mathrm{P}k}P_{\mathrm{PCC}k} + \Omega_k \tag{12}$$

where Ω_k consists of frequency control part $e_{\omega k}$ and active power sharing control part $e_{\mathrm{p}k}$, which satisfies

$$\Omega_k = e_{\omega k} + e_{\mathrm{p}k} \tag{13}$$

The updating laws of $e_{\omega k}$ and $e_{\mathrm{p}k}$ are based on the distributed cooperative control theory and given as

$$\dot{e}_{\omega k} = c_{\omega k}\left[\sum\nolimits_{l\in\mathcal{H}_k} a_k\left(\omega_{\mathrm{MG}l} - \omega_{\mathrm{MG}k}\right) + g_k\left(\omega^*_{\mathrm{sys}} - \omega_{\mathrm{MG}k}\right)\right] \tag{14}$$

$$\dot{e}_{\mathrm{p}k} = c_{\mathrm{p}k}\sum\sum\nolimits_{l\in\mathcal{H}_k} a_k\left(D_{\mathrm{P}l}P_{\mathrm{PCC}l} - D_{\mathrm{P}k}P_{\mathrm{PCC}k}\right) \tag{15}$$

where $c_{\omega k}$ and $c_{\mathrm{p}k}$ are positive control gains, the pinning gain $g_k \geq 0$ is the weight of the edge by which the k_{th} MG unit is connected to the reference. Eq. (14) is applied to synchronize the frequency $\omega_{\mathrm{MG}k}$ of all MGs to the reference ω^*_{sys} to achieve objective (i). Similarly, objective (iii)-(1) will be realized by making $D_{\mathrm{P}k}P_{\mathrm{PCC}k}$ of all MGs equal, as indicated by (15). Note that $\omega_{\mathrm{MG}k}$ is provided to the DSC of MG_k as the frequency reference.

The *critical bus voltage controller* of DQC level is responsible for realizing objective (ii). A control variable λ_k is added in (10), i.e.,

$$\hat{V}_{\mathrm{PCC}k} = V_{\mathrm{n}} - D_{\mathrm{Q}k}Q_{\mathrm{PCC}k} + \lambda_k \tag{16}$$

The updating law of λ_k is given by

$$\dot{\lambda}_k = c_{\mathrm{v}k}[\sum\nolimits_{l\in\mathcal{H}_k} a_{kl}\left(\hat{V}_{\mathrm{PCC}l} - \hat{V}_{\mathrm{PCC}k}\right) + g_k\left(V^*_{\mathrm{f}} - \hat{V}_{\mathrm{PCC}k}\right)] \tag{17}$$

where $c_{\mathrm{v}k}$ is a positive control gain. The dynamic process of (17) results in $\hat{V}_{\mathrm{PCC}k}$ of all MGs converging to the common reference V^*_{f}. V^*_{f} is generated through a PI controller such that V_{c} recovers to its reference V^*_{c} (objective (ii)), i.e.,

$$V^*_{\mathrm{f}} = V_{\mathrm{n}} + k_{\mathrm{p}}\left(V^*_{\mathrm{c}} - V_{\mathrm{c}}\right) + k_{\mathrm{i}}\int\left(V^*_{\mathrm{c}} - V_{\mathrm{c}}\right)dt \tag{18}$$

where k_{p} and k_{i} are the gains of the PI controller.

The *reactive power controller*of DQC level is introduced to solve the inaccurate reactive power sharing problem introduced by TC and realize objective (iii)-(2). A control variable h_k is added to (16) to achieve accurate reactive power

sharing, i.e.,

$$V^*_{\mathrm{PCC}k} = V_n - D_{\mathrm{Q}k} Q_{\mathrm{PCC}k} + \lambda_k + h_k \tag{19}$$

where $V^*_{\mathrm{PCC}k}$ is generated as the voltage reference of DSC in the MG-control layer, as shown in Fig. 2. Note that $\hat{V}_{\mathrm{PCC}k}$ in (16) is an intermediate variable, and $V^*_{\mathrm{PCC}k}$ is the final value provided to DSC as the reference. This setting aims to realize the objectives of critical bus voltage control and reactive power sharing among MGs simultaneously. h_k is selected by

$$\dot{h}_k = c_{\mathrm{q}k} \sum\nolimits_{l \in L_k} a_{kl} \left(D_{\mathrm{Q}l} Q_{\mathrm{PCC}l} - D_{\mathrm{Q}k} Q_{\mathrm{PCC}k} \right) \tag{20}$$

where c_{qk} is a positive control gain. Eq. (20) is used to make $D_{\mathrm{Q}k} Q_{\mathrm{PCC}k}$ of all MGs equal to each other to achieve objective (iii)-(2).

3) COMPLETE MODEL OF THE MG UNIT

The dynamics of PCs, DSCs, lines and loads of each MG in the MG-control layer have been modeled by (8). Therefore, in the MGC-control layer, each MG is considered as a black box and referred to the MG unit, and its corresponding model is about the dynamics of TCs and DQCs. By linearizing (12), (14)-(17), and (19)-(20) around an operating point, the small-signal dynamic model of MG unit k can be derived as

$$\begin{aligned}\left[\Delta \dot{X}_{\mathrm{MG}k}\right] = {} & A_{\mathrm{MG}k} \left[\Delta X_{\mathrm{MG}k}\right] + B_{\mathrm{MG}k} \left[\Delta v_{\mathrm{bDQ}k}\right] + C_{\mathrm{MG}k} \Delta \omega_{\mathrm{g}} \\ & + \sum\nolimits_{l \in H_k} F_{\mathrm{MG}k} \left[\Delta X_{\mathrm{MG}l}\right] H_{\mathrm{MG}k} \Delta V^*_{\mathrm{f}} \\ & + I_{\mathrm{MG}k} \left[\Delta V_{\mathrm{PCCDQ}k}\right]\end{aligned} \tag{21}$$

where $\Delta v_{\mathrm{bDQ}k}$ is the deviation of MV bus voltage $v_{\mathrm{b}k}$ in the commonDQ-frame, $A_{\mathrm{MG}k}$, $B_{\mathrm{MG}k}$ $C_{\mathrm{MG}k}$, $F_{\mathrm{MG}k}$ and $H_{\mathrm{MG}k}$ are parameter matrices. Note that $F_{\mathrm{MG}k}$ reflects the correlation between unit MG_k and its neighbors MG_l, $l \in H_k$. The state variables of each MG unit are

$$\begin{aligned}\left[\Delta X_{\mathrm{MG}k}\right] = {} & [\Delta \delta_k, \Delta P_{\mathrm{PCC}k}, \Delta Q_{\mathrm{PCC}k}, \Delta \Omega_k, \\ & \Delta \lambda_k, \Delta h_k, \Delta i_{\mathrm{PCCd}k}, \Delta i_{\mathrm{PCCq}k}]^T\end{aligned} \tag{22}$$

where $\Delta i_{\mathrm{PCCd}k}$ and $\Delta i_{\mathrm{PCCq}k}$ represent the deviations of $i_{\mathrm{PCC}k}$ in the DQ-frame.

4) CRITICAL BUS VOLTAGE CONTROLLER MODEL

State ψ is introduced to represent the dynamics of critical bus voltage controller (18), given by

$$\dot{\psi} = V^*_{\mathrm{c}} - V_{\mathrm{c}} \tag{23}$$

where V_{c} is the magnitude which can be represented by v_{cD} and v_{cQ}. By linearizing (18) and (23), the model of the critical bus voltage controller can be obtained, i.e.,

$$\Delta \dot{\psi} = -A_{\mathrm{c}} \left[\Delta v_{\mathrm{cDQ}}\right] \tag{24}$$

$$\Delta V^*_{\mathrm{f}} = -k_{\mathrm{p}} A_{\mathrm{c}} \left[\Delta v_{\mathrm{cDQ}}\right] + k_{\mathrm{i}} \Delta \psi \tag{25}$$

where $\Delta v = \left[\Delta v_{\mathrm{cD}}, \Delta v_{\mathrm{cQ}}\right]^T$, and A_{c} is the parameter matrix.

5) MEDIUM VOLTAGE (MV) NETWORK AND LOAD MODELS

The RL feeder lines and the RL-type constant-impedance load are assumed in this paper. The small-signal dynamic model of MV network and load is similar to the LV network and load model in [29], and it can be derived as

$$\Delta \dot{i}_{\mathrm{lineDQ}} = A_{\mathrm{net}} \left[\Delta i_{\mathrm{lineDQ}}\right] + B_{\mathrm{net}} \left[\Delta v_{\mathrm{bDQ}}\right] + C_{\mathrm{net}} \Delta \omega_{\mathrm{g}} \tag{26}$$

$$\Delta \dot{i}_{\mathrm{loadDQ}} = A_{\mathrm{load}} \left[\Delta i_{\mathrm{loadDQ}}\right] + B_{\mathrm{load}} \left[\Delta v_{\mathrm{bDQ}}\right] + C_{\mathrm{load}} \Delta \omega_{\mathrm{g}} \tag{27}$$

where $\Delta i_{\mathrm{lineDQ}}$, $\Delta i_{\mathrm{loadDQ}}$ and Δv_{bDQ} are deviations of all MV line currents, load currents and bus voltages, respectively. $\Delta i_{\mathrm{PCCDQ}}$ denotes $\Delta i_{\mathrm{PCCDQ}k}$ of all the MG units. Then MV bus voltage deviations Δv_{bDQ} is represented as [29]

$$\begin{aligned}\Delta v_{\mathrm{bDQ}} = {} & R_N (M_{\mathrm{MG}} \left[\Delta i_{\mathrm{PCCDQ}}\right] + M_{\mathrm{net}} \left[\Delta i_{\mathrm{lineDQ}}\right] \\ & + M_{\mathrm{load}} \left[\Delta i_{\mathrm{loadDQ}}\right])\end{aligned} \tag{28}$$

Based on (28), the critical bus voltage Δv_{cDQ} can be expressed in terms of $\Delta i_{\mathrm{PCCDQ}}$, $\Delta i_{\mathrm{lineDQ}}$ and $\Delta i_{\mathrm{loadDQ}}$ and named as Δv_{cDQ}*expression*.

6) COMPLETE MGC LAYER MODEL

Denote the state variables of all MG units in the MGC as ΔX_{MG}. Combine (21), (24), (26), (27) and replace$\Delta \mathrm{V}^*_{\mathrm{f}}$, Δv_{bDQ}, $\Delta v_{\mathrm{cDQ}}$with (25), (28) andΔV_{cDQ} expression. Then, the small-signal dynamic model of the MGC-control layer can be obtained, which is

$$\left[\Delta \dot{S}_{\mathrm{MGC}}\right] = A_{\mathrm{MGC}} \left[\Delta S_{\mathrm{MGC}}\right] + B_{\mathrm{MGC}} \Delta V_{\mathrm{PCCDQ}k} \tag{29}$$

where $\Delta S_{\mathrm{MGC}} = [\Delta X_{\mathrm{MG}}, \Delta \psi, \Delta i_{\mathrm{lineDQ}}, \Delta i_{\mathrm{loadDQ}}]^T$, A_{MGC}, B_{MGC} are parameter matrices.

D. COMPLETE SMALL-SIGNAL DYNAMIC MODEL OF THE MGC

By combining m MG-control layer models (8) and MGC-control layer model (29) and then dealing with the coupling states $\Delta V^*_{\mathrm{PCC}k}$, $\Delta i_{\mathrm{PCCDQ}k}$ and $\Delta V_{\mathrm{PCCDQ}k}$, the complete MGC model can be obtained as

$$\left[\Delta \dot{S}_{\mathrm{sys}}\right] = A_{\mathrm{sys}} \left[\Delta S_{\mathrm{sys}}\right] \tag{30}$$

where $\Delta S_{\mathrm{sys}} = [\Delta S_{\mathrm{MG1}}, \ldots, \Delta S_{\mathrm{MG}m}, \Delta S_{\mathrm{MGC}}]^T$.

The system dynamics and stability can be evaluated based on the state matrix A_{sys} in (30), as given in Section III.

III. SMALL-SIGNAL STABILITY ANALYSIS

A detailed small-signal stability analysis of the test 40-bus MGC with four identical LV MGs, as shown in Fig.3, is presented in this section. The MGC is operated as an electrical island, i.e. circuit breaker (CB) is open and CB_1-CB_4 are closed. The MV bus with critical load1 shown in Fig.3 is selected as the critical bus. The rated voltages of MV and LV network are 10kV and 0.38kV, respectively. Each MG connects with the MV feeder through a 10kV/0.38kV $\Delta/\mathrm{Y_g}$ transformer. The corresponding electrical parameters and

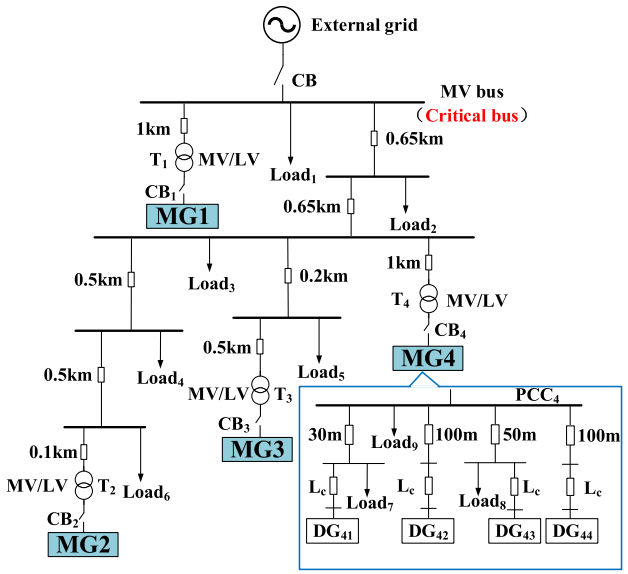

FIGURE 3. A schematic diagram of the test 40-bus MGC.

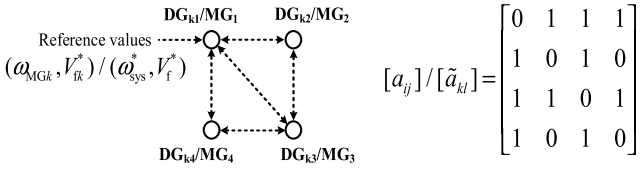

FIGURE 4. Topology of the communication network G_k and $\tilde{G}$.

control parameters are given in Appendix. Fig. 4 shows the communication networks of MG-control layer and MGC-control layer, which are assumed to have the same topology and adjacency matrix. From Fig.4, only one root node receives reference values.

A. SMALL-SIGNAL DYNAMIC MODEL VALIDATION BASED ON TIME-DOMAIN SIMULATION

Based on the aforementioned typical 40-bus MGC, a time-domain validation of the small-signal dynamic model (solid line) against the non-linear model (dashed line) established

in PSCAD/EMTDC is presented in Fig.5. Load 1 suffers a step change from 150kW + 45kVar to 175kW + 65kVar at t = 2s.

The good agreement between the solid line and dashed line in terms of frequency, voltage, active and reactive power in Fig.5 demonstrates the accuracy and the validity of the small-signal dynamic model. The small differences during the transient are mainly due to the linearization error and the ignorance of voltage and current controller, Fig.2, in the modeling process.

B. INFLUENCE OF INTERCONNECTING MGS ON SYSTEM STABILITY

1) THE IMPACT OF INTERCONNECTION OF MG

As illustrated in Section II, the tertiary control is responsible for interconnecting MGs as an islanded MGC. Fig. 6 presents

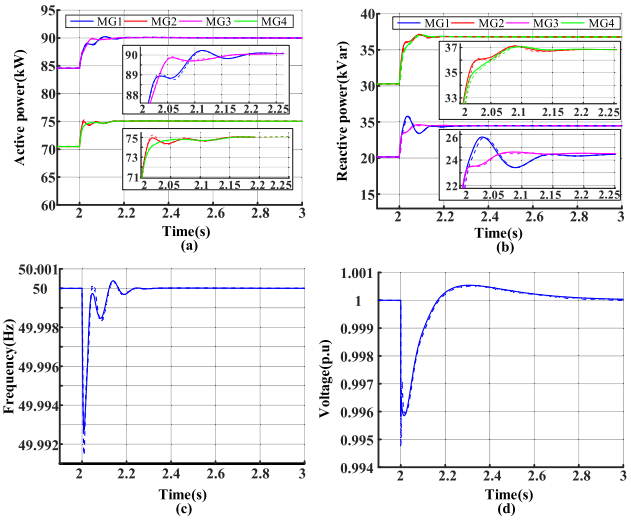

FIGURE 5. Comparison results between non-linear model (dashed line) and small-signal dynamic model (solid line). (a) Active power outputs of MG1-MG4. (b) Reactive power outputs of MG_1-MG_4. (c) System frequency. (d) Critical bus voltage.

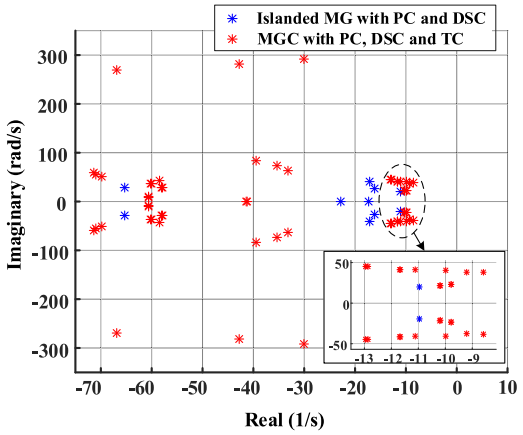

FIGURE 6. Comparison of eigenvalue spectrums of a single MG (with PC and DSC) and a MGC (with PC, DSC, and TC).

the comparison of eigenvalue spectrums between a single MG and the MGC in Fig. 3. Note that (i) the single MG is employed with PC and DSC and operated as an island, and (ii) the MGC consists of four single MGs with PC and DSC which are interconnected with each other through TC level.

Fig.6 indicates that the interconnection of MGs through TC will complicate the system dynamic behavior and reduce the system stability margin.

2) THE IMPACT OF DISTRIBUTED QUATERNARY CONTROL LEVEL

Based on the tertiary control, the distributed quaternary control is introduced to realize frequency, critical bus voltage and accurate power sharing objectives among MGs, as described at Section II. However, the neighboring communication and distributed control algorithm may further deteriorate the system dynamic performance. Fig. 7 presents a comparison of

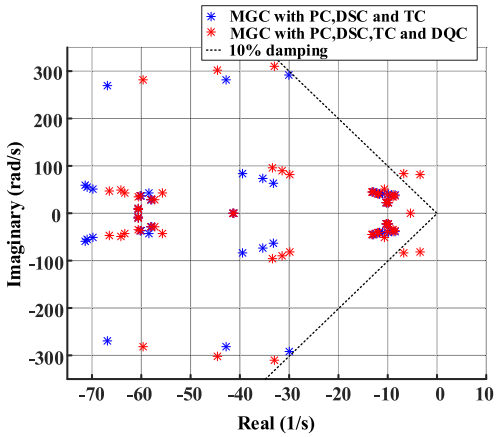

FIGURE 7. Comparison of eigenvalue spectrums of the MGC with and without the DQC control level.

eigenvalue spectrums of the MGC with and without the DQC control level.

The results indicate that the distributed quaternary control introduces two low-damping modes with damping lower than 10%, which will significantly reduce the system stability margin and yield more oscillatory system response.

Comprehensively considering both Fig. 6 and Fig. 7, it can be deduced that interconnection of MGs and the two-layer distributed control method may lead to oscillations even if the sub-MGs are individually stabilized.

C. PARTICIPATION FACTOR ANALYSIS

Participation factor is the multiplication of the corresponding element in the right and left eigenvectors of the state matrix to measure the association between the state variables and the modes. Let ρ_{ki} denote the participation factor of the state variable x_k in mode i, and $\boldsymbol{\rho}_{\mathbf{i}} \in \mathbb{R}^n$ be the vector with the participation factor for all the states of MGC, namely ΔS_{sys}. Similarly, $\boldsymbol{\rho}_{\mathbf{MG_k,i}} \in \mathbb{R}^{n_k}$ is the participation factor vector of all the states of MG_k ($\Delta S_{\text{MG}k}$). $\boldsymbol{\rho}_{\mathbf{MGC,i}} \in \mathbb{R}^{n_{NMG}}$ is the participation factor vector of all the states of the MGC layer (ΔS_{MGC}).

1) MEASUREMENT INDEX OF THE COUPLING DEGREE

Interconnection of MGs and the two-layer distributed control method result in the dynamic coupling among multiple MGs and different control layers. To reveal the relationship between coupling and stability, a quantitative index of coupling degree is proposed.

The index $C_{layer,i}$ aims at describing the coupling degree between the MG and MGC control layers in mode i. First, a participation degree factor $\eta_{MG,i}$ is defined as a measure of the overall participation for MG-control layer states in mode i such that

$$\eta_{MG,i} = \frac{\sum_{k=1}^{m} \left\| \rho_{MG_k,i} \right\|}{\left\| \rho_i \right\|} \tag{31}$$

where $\|\cdot\|$ denotes the L_1-norm. Similarly, the overall participation for MGC-control layer states in mode i is defined as

$$\eta_{MGC,i} = \frac{\sum_{k=1}^{m} \left\| \rho_{MGC,i} \right\|}{\left\| \rho_i \right\|} \tag{32}$$

Obviously, $\eta_{MG,i} + \eta_{MGC,i} = 1$. We define that when the MG-control layer and MGC-control layer states have a fair participation, namely $\eta_{MG,i} = \eta_{MGC,i} = 0.5$, the coupling degree is the strongest. Therefore, $C_{layer,i}$ is defined as

$$C_{layer,i} = \frac{\sqrt{\eta_{MG,i} \times \eta_{MGC,i}}}{(\eta_{MG,i} + \eta_{MGC,i})/2} \tag{33}$$

where $\sqrt{\eta_{MG,i} \times \eta_{MGC,i}}$ implies a penalty. The more deviations from 0.5 of $\eta_{MG,i}$ or $\eta_{MGC,i}$, the smaller this value is. Obviously, $C_{layer,i} \in [0, 1]$ and the larger the value is, the stronger the MG and MGC layer couples.

The coupling degree among MGs is quantified by another index $C_{MG,i}$. The participation degree factor $\eta_{MGk,i}$ represents participation of MG_k in MG layer, given by

$$\eta_{MGk,i} = \frac{\left\| \rho_{MGk,i} \right\|}{\sum_{k=1}^{m} \left\| \rho_{MGk,i} \right\|} \tag{34}$$

Due to $\sum_{k=1}^{m} \eta_{MGk,i} = 1$, we define that (i) when each MG has a fair participation, namely $\eta_{MG1,i} = \eta_{MG2,i} = \ldots = \eta_{MGm,i} = \frac{1}{m}$, the coupling is the strongest, and (ii) when only one arbitrary MG_k participates in mode i, namely $\eta_{MGk,i} = 1$, the coupling is the weakest.

Therefore, $C_{MG,i}$ is defined as

$$C_{MG,i} = 1 - \frac{m^m}{m-1} \times \prod_{k=1}^{m} \left| \eta_{MGk,i} - \frac{1}{m} \right| \tag{35}$$

$\prod_{k=1}^{m} \left| \eta_{MGk,i} - \frac{1}{m} \right|$ means that the more deviations from $\frac{1}{m}$ of $\eta_{MGk,i}$, the smaller this value is. Obviously, $C_{MG,i}$ will be 1 in the strongest coupling situation. The scaling factor $\frac{m^m}{m-1}$ is applied to convert $C_{MG,i}$ to be 0 in the weakest coupling situation.

Then, the comprehensive coupling degree index C_i considering layer coupling $C_{layer,i}$ and MG coupling $C_{MG,i}$ is defined as

$$C_i = 0.5 \times C_{layer,i} + 0.5 \times C_{MG,i} \tag{36}$$

2) PARTICIPATION FACTOR ANALYSIS

The low-frequency eigenvalue spectrum of the test MGC considering the two-layer distributed control strategy is shown in Fig.8. Table 1 provides the dominant low-frequency modes, which are categorized as group A, B, C, and D according to their damping.

TABLE 1. Dominant low-frequency modes and corresponding damping ratios.

Group	A	B	C	D
Damping	<0.1	0.1~0.2	0.2~0.4	0.4~0.8

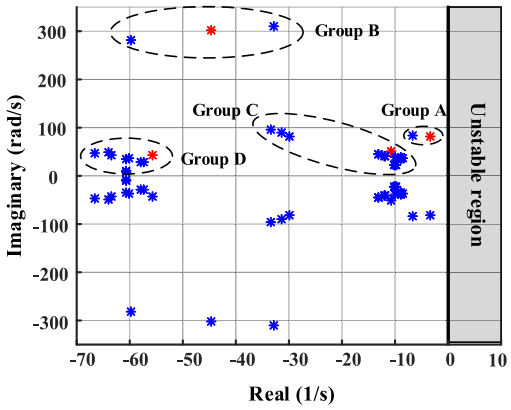

FIGURE 8. Low-frequency eigenvalue spectrum of the MGC.

Modes 1, 2, 3 and 4 are *respectively* selected as the representative modes of group A, B, C, and D and*marked with red* in Fig. 8. Their corresponding participation factors of the system state variables are shown in Fig. 9. Participation factors of other modes are similar to the corresponding representative modes and thus not presented. Fig.10 shows the damping ratio ζ_i and coupling degree C_i of modes $1 \sim 4$. The analysis results of Fig.9 and Fig.10 are summarized as follows.

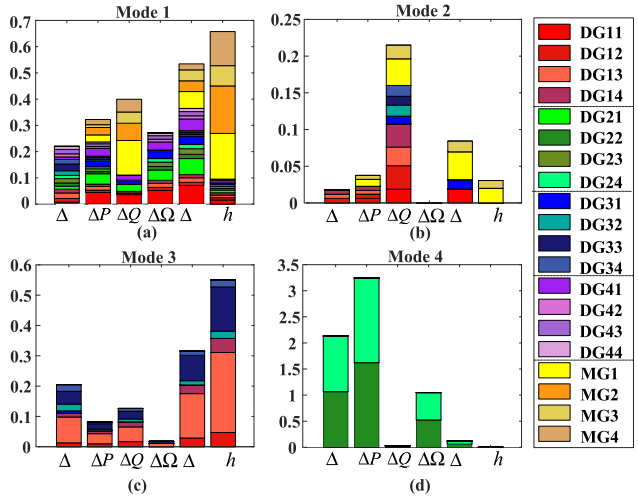

FIGURE 9. Participation factors of modes 1, 2, 3 and 4.

(i) Modes 1,2,3 are inter-MG modes which means these modes are associated with multiple MGs as shown in Fig. 9 (a), (b), and (c). Mode 1 is affected by the states of $MG_1 \sim MG_4$ and mode 2 is associated with MG_1 and MG_3. For mode 3, its difference from modes 1 and 2 is that the participation of MGC-control layer further enhances the inter-MG coupling for mode 1 and 2 but not for mode 3. Moreover, Fig. 9(d) indicates that mode 4 is a MG local mode, which is only affected by the states of MG_4.

(ii) The coupling degree has a strong relationship with the mode damping. As indicated in Fig. 10, the stronger the coupling degree is, the less damped the mode is.

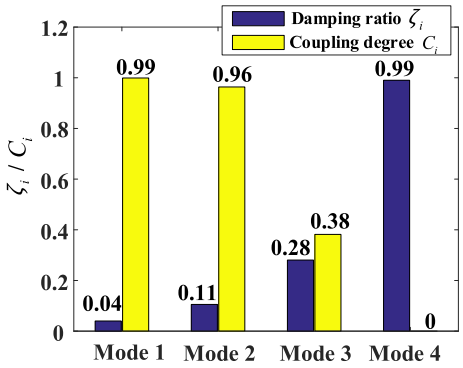

FIGURE 10. Damping ratios and coupling degree of modes 1, 2, 3 and 4.

(iii) Fig.9 indicates that the MG-control layer states $(\Delta\delta_{ki}, \Delta P_{ki}, \Delta Q_{ki}, \Delta\Omega_{ki}, \Delta\lambda_{ki}, \Delta h_{ki})$ and MGC-control layer

states $(\Delta\delta_k, \Delta P_k, \Delta Q_k, \Delta\Omega_k, \Delta\lambda_k, \Delta h_k)$ contribute to modes 1-4 in different proportions. Since the MG-control layer states associate with DSCs and MGC-control layer states associate with DQCs of (14), (15), (17), and (20), the impact of DSC and DQC parameters should be carefully analyzed.

D. IMPACT OF CONTROL PARAMETERS ON SYSTEM STABILITY

In this part, the impacts of control parameters are analyzed in two aspects: (i) ratio of DSC and DQC parameters; (ii) sensitivity analysis of DSC and DQC parameters.

1) IMPACT OF THE RATIO OF DSC AND DQC PARAMETERS

The DSC control parameter $C_{wki}, C_{pki}, C_{vki}, C_{qki}$ are chosen as (500, 50, 20 and 50). Note that C_{wki}, C_{pki} are the parameters of distributed secondary frequency controller, and C_{vki}, C_{qki} are the parameters of distributed secondary voltage controller. More details can be found in [27]. The DQC parameters are set as $C_{wk} = \gamma * C_{wki}, C_{pk} = \gamma * C_{pki}, C_{vk} = \gamma * C_{vki}, C_{qk} = \gamma * C_{qki}$. Fig. 11 presents the traces of low-frequency eigenvalues when γ varies from 0.1 to 5.

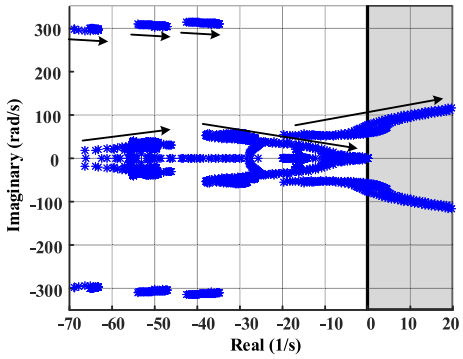

FIGURE 11. Traces of low-frequency eigenvalues when γ varies from 0.1 to 5.

Fig. 11 indicates that a relatively smaller γ leads to a more stable system while a large value of γ may destabilize the system. Therefore, it can be deduced that the interaction between MG-control layer and MGC-control layer has a strong impact on the system stability.

Remark 1: The DSC and DQC parameters are related with the response time of MG and MGC control layer, respectively. Thus, the ratio γ actually describes the time-scale separation degree of the MG and MGC control layer. As shown by the red arrow in Fig. 2, the DSC in MG-control layer tracks the reference values from TC and DQC in MGC-control layer. It should be noted that the time constant of TC is much smaller compared with DQC and thus can be ignored in the response time of MGC-control layer. Therefore, if the reference values from the DQC in MGC-control layer vary too fast, namely the response time of MGC-control layer is much smaller than that of MG-control layer, the DSC cannot follow the references and then the system becomes unstable.

2) SENSITIVITY ANALYSIS OF PARAMETERS ON STABILITY

As shown in Table 1, the damping of modes in group A is less than 10% and therefore identified as the most dominant oscillatory modes. Based on the participation factor analysis, the MG-control layer parameters C_{pki}, C_{vki} and the MGC-control layer parameters C_{vk}, C_{qk} mainly affect modes in group A and thus they are evaluated in this subsection. The traces of modes as a function of C_{pki}, C_{vki}, C_{vk}, C_{qk} are shown in Fig. 12. The red circles are the eigenvalues with initial parameters. Fig.12 (a)-(d) show that the variation of parameters will make the damping of some modes decrease obviously. And eventually, these modes cross the imaginary axis to the unstable region. Thus, proper control parameters should be selected to ensure sufficient damping. However, Fig.12 (b) and (d) indicate that the trend of a parameter may have opposite effects on the damping of different modes, e.g., c_{qk} and c_{vki} on group A and group B. Therefore, a joint parameter selection method considering the impacts of multiple parameters needs to be studied.

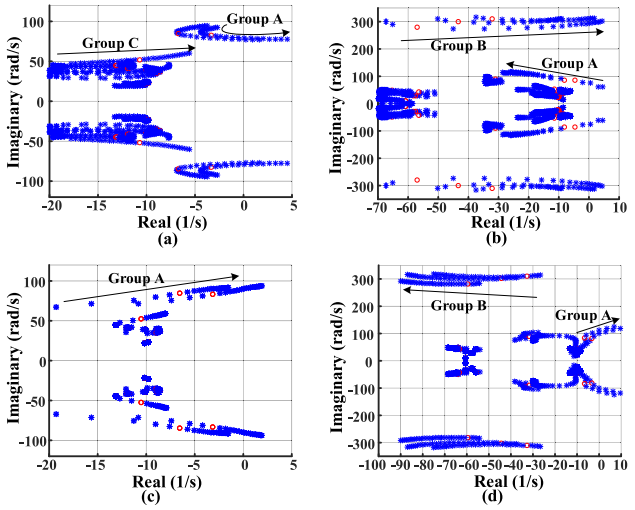

FIGURE 12. Traces of dominant modes. (a) C_{pki} increases from 10 to 200. (b) C_{vki} increases from 10 to 200. (c) C_{vk} increases from 10 to 250. (d) C_{qk} increases from 5 to 150.

E. SUMMARY

THE results in this section reveal that for a MGC with the two-layer distributed control method, (i) the strong coupling/interaction among MGs and multiple control layers will introduce some new low-damping modes, which can reduce the system stability margin and even destabilize the system, (ii) the variation of DSC and DQC parameters will have remarkable impacts on the mode damping, and (iii) a

reasonable selection of control parameters can enhance the system stability. However, the large number of control parameters makes their selection a multi-dimensional optimization problem, which is difficult to obtain an optimal solution. Therefore, there is a need to provide a parameter optimization method to carefully design the control parameters and enhance the system stability.

IV. OPTIMAL DESIGN OF DISTRIBUTED CONTROL PARAMETERS

In this section, the selection of DSC and DQC parameters is formulated as an optimization problem and solved by the particle swarm optimization (PSO) algorithm [30].

A. PROBLEM FORMULATION

In order to enhance the MGC stability margin and damping characteristics, the objective function of the optimization problem aims to (i) move the real part σ of eigenvalues to a relatively far area from the imaginary axis and (ii) increase their damping ratio ζ as much as possible. The comprehensive assessment index J is defined as

$$J = J_{att} + J_{osc} \tag{37}$$

where J_{att} and J_{osc} are assessment indices with respect to attenuation modes and oscillation modes, respectively. Note that the imaginary part of an attenuation mode is zero, and the imaginary part of an oscillation mode is non-zero.

As the damping ratio ζ and real part σ are in different dimensions, they cannot be readily applied in (37). Therefore, variables f_ζ and f_σ are introduced to normalize $|\sigma|$ and ζ within the range of 0 to 1. The normalized function f_x is [31]

$$f_x = 1 - e^{-\frac{1}{\tau}(\mu-\mu_0)}, \mu \geq \mu_0 \tag{38}$$

where μ_0 and τ determine the function as shown in Fig. 13. A pre-specified point (μ_s, 0.95) on the plot of Fig. 13 is used to determine τ for (38), i.e.,

$$\tau = \frac{\mu_0 - \mu_s}{\ln 0.05} \tag{39}$$

Based on (38), $|\sigma|$ and ζ can be normalized as

$$f_{|\sigma_j|} = 1 - e^{-\frac{1}{\tau_{|\sigma_j|}}\left(|\sigma_j| - \mu_{0\_|\sigma_j|}\right)}, \quad |\sigma_j| \geq \mu_{0\_|\sigma_j|} \tag{40}$$

$$f_{\zeta_j} = 1 - e^{-\frac{1}{\tau_{\zeta_j}}\left(\zeta_j - \mu_{0\_\zeta_j}\right)}, \quad \mu \geq \mu_{0\_\zeta_j} \tag{41}$$

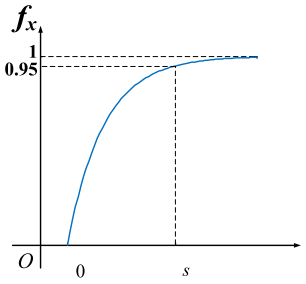

FIGURE 13. Normalization function.

where $f_{|\sigma_j|}$ and f_{ζ_j} are the normalization values for $|\sigma|$ and ζ of mode j. $\mu_{0\_|\sigma_j|}$, $\mu_{0\_\zeta_j}$, $\tau_{|\sigma_j|}$ and τ_{ζ_j} are the corresponding parameters.

Therefore, the assessment indices J_{att} and J_{osc} can be represented as

$$J_{att} = \sum_{\rho=1}^{\alpha} w_\rho f_{|\sigma_\rho|} \tag{42}$$

$$J_{osc} = \sum_{\mu=1}^{\beta} w_\mu (f_{|\sigma_\mu|} + f_{\zeta_\mu}) \tag{43}$$

where α is the total number of attenuation modes, w_ρ is the weighting factor and satisfies $\sum_{\rho=1}^{\alpha} w_\rho = 1$, β is the total number of oscillation modes, and w_μ is the weighting factor and satisfies $\sum_{\mu=1}^{\beta} w_\mu = 1$.

To optimize the system stability margin and damping, index J must be maximized. Therefore, the optimization problem is formulated as

$$\begin{aligned} \max J =& J_{att} + J_{osc} \\ s.t. \begin{cases} |\lambda I - A_{\text{sys}}| = 0, \\ C_{w\_DG}^{min} \le C_{w\_DG} \le C_{w\_DG}^{max}, \\ C_{p\_DG}^{min} \le C_{p\_DG} \le C_{p\_DG}^{max}, \\ C_{v\_DG}^{min} \le C_{v\_DG} \le C_{v\_DG}^{max}, \\ C_{q\_DG}^{min} \le C_{q\_DG} \le C_{q\_DG}^{max}, \\ C_{w\_MG}^{min} \le C_{w\_MG} \le C_{w\_MG}^{max}, \\ C_{p\_MG}^{min} \le C_{p\_MG} \le C_{p\_MG}^{max}, \\ C_{v\_MG}^{min} \le C_{v\_MG} \le C_{v\_MG}^{max}, \\ C_{q\_MG}^{min} \le C_{q\_MG} \le C_{q\_MG}^{max}, \end{cases} \end{aligned} \tag{44}$$

where λ is the eigenvalue of A_{sys}, I is the identity matrix. The control parameters of MG-control layer (C_{wki}, C_{pki}, C_{vki}, C_{qki}) and MGC-control layer (C_{wk}, C_{pk}, C_{vk}, C_{qk}) are chosen as optimization variables. To simplify analysis, the DSC parameters of each DG unit are represented by C_{w_DG}, C_{p_DG}, C_{v_DG}, C_{q_DG}, and the DQC parameters are represented by C_{w_MG}, C_{p_MG}, C_{v_MG}, C_{q_MG}. They are constrained by the corresponding lower limits and upper limits as shown in (44).

B. PSO IMPLEMENTATION

Problem (44) is a non-linear and non-convex optimization problem, which also includes eigenvalues constraints. Thus, PSO is adopted to solve this problem to obtain the optimal distributed control parameters. Fig. 14 depicts the computational flowchart of the method. The overall optimization process can be described in the following steps:

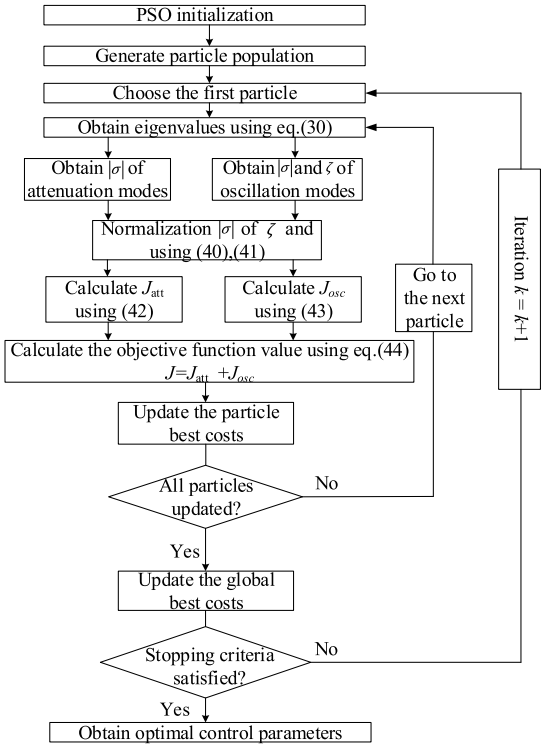

FIGURE 14. Flow chart of the PSO-based distributed control parameter optimization.

Step 1) (Initialization): generate a random particle population and generate randomly initial velocities and positions for each particle.

Step 2) (Obtain Eigenvalues): choose the first particle and calculate the corresponding eigenvalues via matrix A_{sys} in (30). Note that the position vector of each particle consists of DSC and DQC parameters.

Step 3) (Obtain σ and ζ and Normalization): obtain the real part σ of attenuation modes and oscillation modes, and calculate the damping ratio ζ of the oscillation modes. Then, normalize σ and ζ by (40) and (41), respectively.

Step 4) (Calculate J for Each Particle i at Iteration k): calculate $J_{att,i}^k$ and $J_{osc,i}^k$ by (42) and (43), respectively. Then, the final objective function J_i^k can be obtained by (44).

Step 5) (Individual Best Updating): update J_i^k for each particle in the population. If $J_i^k > J_{i,best}$, then update the individual best $J_{i,best} = J_i^k$ and go to the next step; else do not update and go to the next step.

Step 6) (Global Best Updating): Search for the maximum value J_{max} among the individual best $J_{i,best}$. If $J_{max} > J_{g,best}$,

then update global best as $J_{g,best} = J_{max}$ and go to the next step; else do not update and go to the next step.

Step 7) (Stopping Criteria): The search process will be terminated if the number of iterations is greater than a pre-specified number.

V. CASE STUDY

To evaluate the proposed optimal parameter design method, stability assessment and time-domain simulation studies in the PSCAD/EMTDC platform are carried out based on the 40-bus MGC shown in Fig. 3 and Fig. 4. The parameters are given in Appendix.

A. STABILITY ASSESSMENT

Based on the optimal design method introduced at Section IV, the MG-control layer and MGC-control layer parameters are optimized and the results are given in Appendix. The convergence performance of the PSO method, shown in Fig. 15, indicates that the objective value converges to the maximum value 2.61 around the 20th iteration, which shows a good convergence performance of the PSO based method.

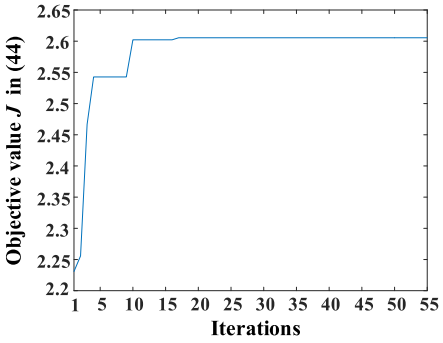

FIGURE 15. Convergence result of the PSO-based distributed control parameter optimization.

1) COMPARISON OF EIGENVALUE SPECTRUM BEFORE AND AFTER OPTIMIZATION

The low-frequency eigenvalue spectrum of the MGC before and after optimization is compared in Fig. 16.

Fig. 16 indicates that after optimization, (i) the damping ratios of the system critical oscillatory modes are increased, and (ii) the critical system eigenvalues move further away from the imaginary axis.

2) COMPARISON OF COUPLING DEGREE BEFORE AND AFTER OPTIMIZATION

The average coupling degree of the five least-damped modes is defined as C_{ave} and the coupling degree of the least damped mode is defined asC_l. The comparison of C_{ave} and C_l before and after optimization is given in Table 2.

Table 2 indicates that the coupling degrees of the low-damping modes are significantly reduced after optimization. Considering the result of Fig.16, it can be deduced that the damping ratios of the low-damping modes are enhanced due to the decreased coupling degree.

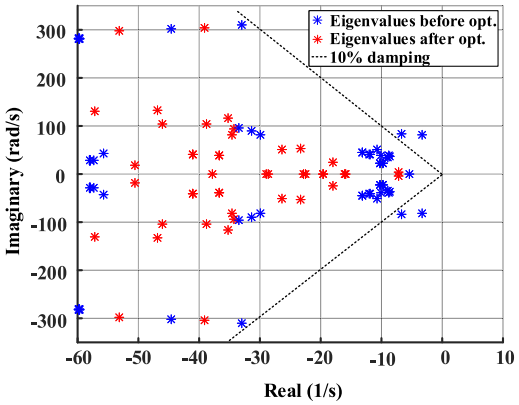

FIGURE 16. Comparison of eigenvalue spectrum before and after optimization.

TABLE 2. Coupling degree comparison before and after optimization.

	Before optimization	After optimization
C_{ave}	0.9403	0.5654
C_l	0.9992	0.9395

B. TIME-DOMAIN SIMULATION RESULTS

This subsection is organized into two studies. Study 1 evaluates the stability enhancement effect with the optimally designed two-layer distributed controllers. Study 2 validates the robustness of the proposed method under sudden load changes.

1) STUDY 1: STABILITY ENHANCEMENT EVALUATION

The PCs are initially engaged and the DSCs and TCs are activated at t = 1.5s. DQCs are employed at t = 3s. Fig. 17 and Fig. 18 present the active and reactive power outputs of MGs and DGs under initial control parameters and

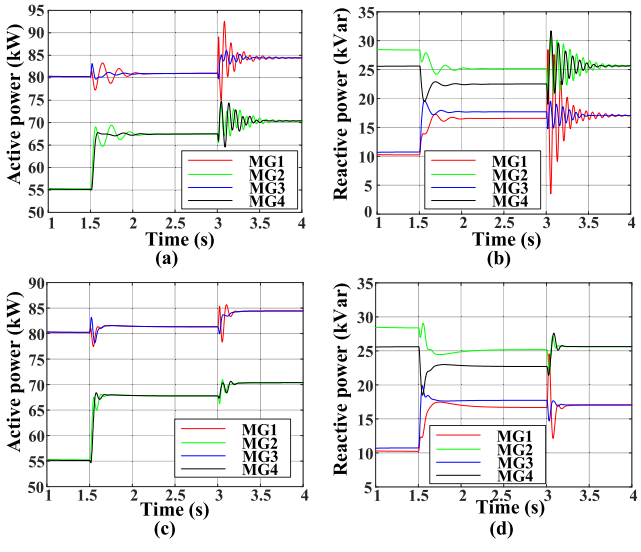

FIGURE 17. Study 1: active and reactive output of MG_1-MG_4. (a) and (b): before optimization; (c) and (d): after optimization.

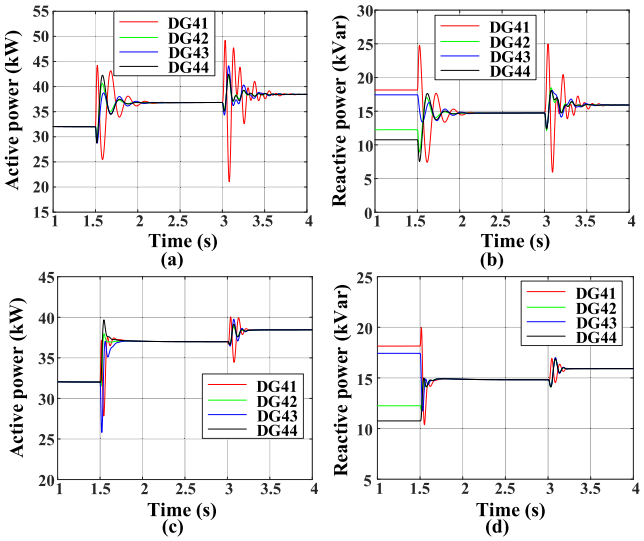

FIGURE 18. Study 1: Active and reactive output of DG_{41}-DG_{44} in MG_4. (a) and (b): before optimization; (c) and (d): after optimization.

optimal control parameters, respectively. Note that only the output power of DGs in MG_4 is presented for simplification. Fig. 19 shows the comparison results of system frequency and critical bus voltage. Comparisons of Fig. 17, 18 and 19 reveal that the system stability is enhanced by the optimally designed control parameters.

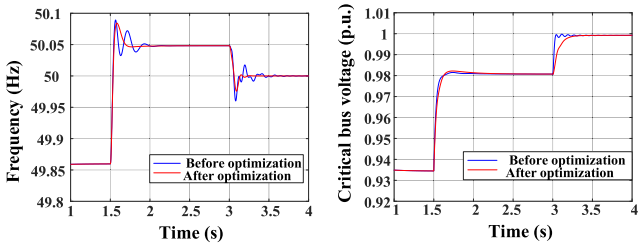

FIGURE 19. Study 1: System frequency and critical bus voltage before and after optimization.

Moreover, considering the four control objectives in Section II, Fig. 17, 18, and 19 indicate that the optimal design of control parameter does not interfere with the system steady-state performance, because the control strategy can achieve objective (i): restoration of the system frequency to the rated value 50 Hz, Fig. 19(a), objective (ii): restoration of the PCC voltage to the rated value 1 p.u., Fig. 19(b), objective (iii): accurate active and reactive power sharing among MGs with the ratios of P_{PCC1} to P_{PCC4} being 1.2:1:1.2:1 and Q_{PCC1} to Q_{PCC4} being 1:1.5:1:1.5, Fig. 17 (c) and (d), and objective (iv): accurate active and reactive power sharing among DGs within $MG_4$with the ratios of P_{41} to P_{44} being 1:1:1:1 and Q_{41} to Q_{41} being 1:1:1:1, Fig. 18 (c) and (d).

Remark 2: with the optimal control parameters, the overshoot of active and reactive power responses is decreased and the corresponding settling time is decreased. However, due to the coupling/interaction among MGs and multiple control layers, a certain degree of oscillation still exists. A possible way to further mitigate the oscillation is to introduce supplementary controllers. This is beyond the scope of this paper and will be investigated in future work.

2) STUDY 2: SUDDEN LOAD CHANGE

To evaluate the system dynamic performance when suffering sudden load changes, 50% of load 1 is switched off at t = 2.5s and load 7 is switched off at t = 3.5s. The reactive power outputs of MGs under initial control parameters and optimal control parameters are presented in Fig. 20 (a) and (b), respectively. The reactive power outputs of DGs in MG_4 under initial control parameters and optimal control parameters are presented in Fig. 21 (a) and (b), respectively.

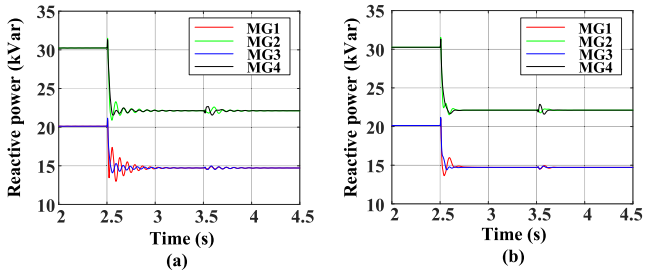

FIGURE 20. Study 2: reactive power outputs of all the MGs (a) before and (b) after optimization.

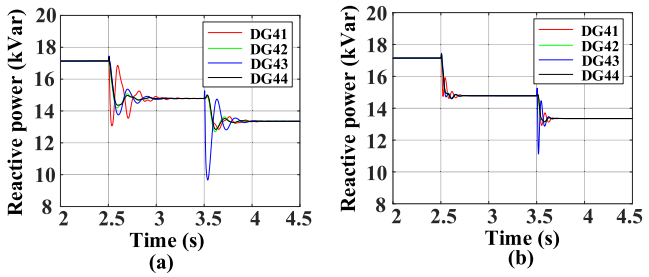

FIGURE 21. Study 2: reactive power outputs of all the DGs in MG_4 (a) before and (b) after optimization.

Comparisons in Fig. 20 and 21 indicate that the controller with optimal parameters can mitigate the oscillations and improve the system stability, which validates the robustness of the controllers with optimal parameters under significant load changes.

VI. CONCLUSIONS

This paper presents a detailed small-signal stability analysis and optimal control parameters design method for MGC with the two-layer distributed control strategy. The small-signal stability analysis reveals that (i) the interconnection of MGs and the neighboring communication of distributed control algorithm may introduce new low-damping modes to the system, (ii) the coupling degree of a mode has an opposite relationship with its damping ratio, (iii) the mode damping is affected by multiple parameters of both MG and MGC control layer. Based on the small-signal dynamic model, the design of MG and MGC layer control parameters is formulated as an optimization problem and the optimal control parameters are solved by PSO algorithm. Eigenvalue analysis and

time-domain simulation on a test MGC system validate that with the proposed optimal control parameter design method, the stability performance of the MGC is improved.

APPENDIX

Table 3 provides the electrical parameters of the test MGC in Fig. 3. Table 4 provides the parameters of PCs and TCs. Tables 5 and 6 provide the control parameters of DSCs and DQCs before and after optimization, respectively.

TABLE 3. Electrical parameters of MGC.

Line	**MV line:** 0.069+j0.099Ω **LV line:** 0.284+j0.083Ω
Load	**MV load:** $Load_1$=150kw+45kvar, $Load_2$=25kw+7.5kvar, $Load_3$=75kw+22.5kvar, $Load_{4,5,6}$=20kw+5 kvar. **LV load:** $Load_7$=15kw+7.5kvar,$Load_8$=12kw+5kvar, $Load_9$=50kw+20kvar.
Transformer	T_1~T_4: 1MVA, $u_k = 4\%$, $r_k = 1\%$, 10/0.38KV(Δ/Y_g)
Coupling inductance	L_c=0.1mH

TABLE 4. Parameters of PCs and TCs.

Parameters	DGs in MG_1 and MG_3	DGs in MG_2 and MG_4	MG_1 MG_3	MG_2 MG_4
D_{Pki}/D_{Pk} (Hz/kW · 10^{-3})	16.67	20	5.56	6.67
D_{Qki}/D_{Qk} (kV/kvar · 10^{-3})	0.7775	0.5183	0.26	0.173
P_{max}/P_{sMG} (kW)	60	50	120	100
Q_{max}/Q_{sMG} (kvar)	20	30	40	60

TABLE 5. Parameters of DSCs and DQCs before optimization.

Parameters	DSC level	DQC level
$c_{\omega ki}/c_{\omega k}$	490	3018
c_{pki}/c_{pk}	85	3243
c_{vki}/c_{vk}	28	58
c_{qki}/c_{qk}	10	26

TABLE 6. Parameters of DSCs and DQCs after optimization.

Parameters	DSC level	DQC level
$c_{\omega ki}/c_{\omega k}$	550	2530
c_{pki}/c_{pk}	45	2640
c_{vki}/c_{vk}	20	15
c_{qki}/c_{qk}	90	23

REFERENCES

[1] N. Hatziargyriou, H. Asano, R. Iravani, and C. Marnay, "Microgrids," *IEEE Power Energy Mag.*, vol. 5, no. 4, pp. 78–94, Jul./Aug. 2007.
[2] F. Katiraei and M. R. Iravani, "Power management strategies for a microgrid with multiple distributed generation units," *IEEE Trans. Power Syst.*, vol. 21, no. 4, pp. 1821–1831, Nov. 2006.
[3] R. H. Lasseter and P. Paigi, "Microgrid: A conceptual solution," in *Proc. IEEE 35th Annu. Power Electron. Spec. Conf.*, Aachen, Germany, Jun. 2004, pp. 4285–4290.
[4] S. Moayedi and A. Davoudi, "Distributed tertiary control of DC microgrid clusters," *IEEE Trans. Power Electron.*, vol. 31, no. 2, pp. 1717–1733, Feb. 2016.
[5] Y. Xu, C.-C. Liu, K. P. Schneider, F. K. Tuffner, and D. T. Ton, "Microgrids for service restoration to critical load in a resilient distribution system," *IEEE Trans. Smart Grid*, vol. 9, no. 1, pp. 426–437, Jan. 2018.
[6] J. M. Guerrero, J. C. Vasquez, J. Matas, L. G. de Vicuna, and M. Castilla, "Hierarchical control of droop-controlled AC and DC microgrids—A general approach toward standardization," *IEEE Trans. Ind. Electron.*, vol. 58, no. 1, pp. 158–172, Jan. 2011.
[7] D. E. Olivares *et al.*, "Trends in microgrid control," *IEEE Trans. Smart Grid*, vol. 5, no. 4, pp. 1905–1919, Jul. 2014.
[8] G. Liu, M. R. Starke, B. Ollis, and Y. Xue. (Oct. 2016). *Networked Microgrids Scoping Study*. ORNL. [Online]. Available: https://info.ornl.gov/sites/publications/files/Pub68339.pdf
[9] X. Lu, J. Lai, X. Yu, Y. Wang, and J. M. Guerrero, "Distributed coordination of islanded microgrid clusters using a two-layer intermittent communication network," *IEEE Trans. Ind. Informat.*, vol. 14, no. 9, pp. 3956–3969, Sep. 2018.
[10] J. Lopes, A. Madureira, N. Gil, and F. Resende, "Operation of multimicrogrids," in *Microgrids Architecture and Control*. Chichester, U.K.: Wiley, 2014.
[11] I. U. Nutkani, P. C. Loh, and F. Blaabjerg, "Distributed operation of interlinked AC microgrids with dynamic active and reactive power tuning," *IEEE Trans. Ind. Appl.*, vol. 49, no. 5, pp. 2188–2196, Sep. 2013.
[12] B. Huang, Y. Li, H. Zhang, and Q. Sun, "Distributed optimal co-multimicrogrids energy management for energy Internet," *IEEE/CAA J. Automatica Sinica*, vol. 3, no. 4, pp. 357–364, Oct. 2016.
[13] M. S. Golsorkhi, D. J. Hill, and H. R. Karshenas, "Distributed voltage control and power management of networked microgrids," *IEEE Trans. Emerg. Sel. Topics Power Electron.*, vol. 6, no. 4, pp. 1892–1902, Dec. 2018.
[14] J. Zhou, H. Zhang, Q. Sun, D. Ma, and B. Huang, "Event-based distributed active power sharing control for interconnected AC and DC microgrids," *IEEE Trans. Smart Grid*, vol. 9, no. 6, pp. 6815–6828, Nov. 2018.
[15] W. Liu, W. Gu, Y. Xu, Y. Wang, and K. Zhang, "General distributed secondary control for multi-microgrids with both PQ-controlled and droop-controlled distributed generators," *IET Gener., Transmiss. Distrib.*, vol. 11, no. 3, pp. 707–718, Feb. 2017.
[16] Y. Zhang, L. Xie, and Q. Ding, "Interactive control of coupled microgrids for guaranteed system-wide small signal stability," *IEEE Trans. Smart Grid*, vol. 7, no. 2, pp. 1088–1096, Mar. 2016.
[17] Z. Zhao, P. Yang, Y. Wang, Z. Xu, and J. M. Guerrero, "Dynamic characteristics analysis and stabilization of PV-based multiple microgrid clusters," *IEEE Trans. Smart Grid*, vol. 10, no. 1, pp. 805–818, Jan. 2019.
[18] M. A. Hassan and M. A. Abido, "Optimal design of microgrids in autonomous and grid-connected modes using particle swarm optimization," *IEEE Trans. Power Electron.*, vol. 26, no. 3, pp. 755–769, Mar. 2011.
[19] I. Chung, W. Liu, D. A. Cartes, E. G. Collins, and S. Moon, "Control methods of inverter-interfaced distributed generators in a microgrid system," *IEEE Trans. Ind. Appl.*, vol. 46, no. 3, pp. 1078–1088, May/Jun. 2010.
[20] I. Ngamroo and S. Vachirasricirikul, "Design of optimal SMES controller considering SoC and robustness for microgrid stabilization," *IEEE Trans. Appl. Supercond.*, vol. 26, no. 7, Oct. 2016, Art. no. 5403005.
[21] K. Yu, Q. Ai, S. Wang, J. Ni, and T. Lv, "Analysis and optimization of droop controller for microgrid system based on small-signal dynamic model," *IEEE Trans. Smart Grid*, vol. 7, no. 2, pp. 695–705, Mar. 2016.
[22] R. Olfati-Saber, J. A. Fax, and R. M. Murray, "Consensus and cooperation in networked multi-agent systems," *Proc. IEEE*, vol. 95, no. 1, pp. 215–233, Jan. 2007.
[23] W. Ren, R. W. Beard, and E. M. Atkins, "Information consensus in multivehicle cooperative control," *IEEE Control Syst. Mag.*, vol. 27, no. 2, pp. 71–82, Apr. 2007.
[24] A. Bidram, A. Davoudi, F. L. Lewis, and Z. Qu, "Secondary control of microgrids based on distributed cooperative control of multi-agent systems," *IET Generat., Transmiss., Distrib.*, vol. 7, no. 8, pp. 822–831, Aug. 2013.
[25] M. C. Chandorkar, D. M. Divan, and R. Adapa, "Control of parallel connected inverters in standalone AC supply systems," *IEEE Trans. Ind. Appl.*, vol. 29, no. 1, pp. 136–143, Jan./Feb. 1993.

[26] J. M. Guerrero, L. Garcia de Vicuna, J. Matas, M. Castilla, and J. Miret, "Output impedance design of parallel-connected UPS inverters with wireless load-sharing control," *IEEE Trans. Ind. Electron.*, vol. 52, no. 4, pp. 1126–1135, Aug. 2005.
[27] X. Wu, C. Shen, and R. Iravani, "A distributed, cooperative frequency and voltage control for microgrids," *IEEE Trans. Smart Grid*, vol. 9, no. 4, pp. 2764–2776, Jul. 2018.
[28] Y. W. Li and C.-N. Kao, "An accurate power control strategy for power-electronics-interfaced distributed generation units operating in a low-voltage multibus microgrid," *IEEE Trans. Power Electron.*, vol. 24, no. 12, pp. 2977–2988, Dec. 2009.
[29] N. Pogaku, M. Prodanovic, and T. C. Green, "Modeling, analysis and testing of autonomous operation of an inverter-based microgrid," *IEEE Trans. Power Electron.*, vol. 22, no. 2, pp. 613–625, Mar. 2007.
[30] J. Kennedy and R. Eberhart, "Particle swarm optimization," in *Proc. Int. Conf. Neural Netw. (ICNN)*, Perth, WA, Australia, vol. 4, 1995, pp. 1942–1948.
[31] X. Wu, C. Shen, and R. Iravani, "Feasible range and optimal value of the virtual impedance for droop-based control of microgrids," *IEEE Trans. Smart Grid*, vol. 8, no. 3, pp. 1242–1251, May 2017.

JINGHAN HE (M'07–SM'18) received the M.Sc. degree in electrical engineering from Tianjin University, Tianjin, China, in 1994, and the Ph.D. degree in electrical engineering from Beijing Jiaotong University, Beijing, China, in 2007, where she is currently a Professor. Her main research interests include protective relaying, fault distance measurement, and location in power systems.

XIAOYU WU (S'15) received the B.S. degree in electrical engineering from Beijing Jiaotong University, Beijing, China, in 2013, where he is currently pursuing the Ph.D. degree.

From 2015 to 2016, he was a Visiting Scholar with North Carolina State University, Raleigh, NC, USA. His research interests include demand response, and control and stability analysis of microgrid.

XIANGYU WU (S'13–M'17) received the B.S. degree from the Department of Electrical Engineering, Zhejiang University, Hangzhou, China, in 2012, and the Ph.D. degree in electrical engineering from Tsinghua University, Beijing, China, in 2017.

In 2015, he was a Visiting Scholar with the University of Toronto, Toronto, ON, Canada. Since 2018, he has been a Guest Researcher with the Department of Energy Technology, Aalborg University, Aalborg, Denmark. He is currently a Postdoctoral Researcher with the School of Electrical Engineering, Beijing Jiaotong University, Beijing. His research interests include the control and stability analysis of microgrid and power electronic-based power systems.

YIN XU (S'12–M'14–SM'18) received the B.E. and Ph.D. degrees in electrical engineering from Tsinghua University, Beijing, China, in 2008 and 2013, respectively.

He is currently a Professor with the School of Electrical Engineering, Beijing Jiaotong University, Beijing. From 2013 to 2016, he was an Assistant Research Professor with the School of Electrical Engineering and Computer Science, Washington State University, Pullman, WA, USA. His research interests include power system resilience, distribution system restoration, power system electromagnetic transient simulation, and ac–dc hybrid power systems.

Dr. Xu is currently serving as the Secretary of the Distribution Test Feeder Working Group, IEEE PES Distribution System Analysis Subcommittee.

JOSEP M. GUERRERO (S'01–M'04–SM'08–F'15) received the B.S. degree in telecommunications engineering, the M.S. degree in electronics engineering, and the Ph.D. degree in power electronics from the Technical University of Catalonia, Barcelona, in 1997, 2000, and 2003, respectively.

Since 2014, he has been the Chair Professor with Shandong University. Since 2015, he has been a Distinguished Guest Professor with Hunan University. Since 2016, he has been a Visiting Professor Fellow with Aston University, U.K., and a Guest Professor with the Nanjing University of Posts and Telecommunications. Since 2011, he has been a Full Professor with the Department of Energy Technology, Aalborg University, Denmark, where he is responsible for the Microgrid Research Program. He has published more than 450 journal papers in the fields of microgrids and renewable energy systems, which are cited more than 30 000 times. His research interests include different microgrid aspects, including power electronics, distributed energy-storage systems, hierarchical and cooperative control, energy management systems, smart metering and the Internet of Things for ac/dc microgrid clusters, and islanded minigrids, recently specially focused on maritime microgrids for electrical ships, vessels, ferries, and seaports. In 2015, he was elevated as the IEEE Fellow for his contributions on distributed power systems and microgrids. He received the Best Paper Award of the IEEE TRANSACTIONS ON ENERGY CONVERSION, for the period 2014–2015 and the Best Paper Prize of the IEEE-PES, in 2015. He also received the Best Paper Award of the *Journal of Power Electronics*, in 2016. From 2014 to 2018, he was awarded by Thomson Reuters as the Highly Cited Researcher. He is also an Associate Editor for a number of IEEE TRANSACTIONS.